Tip-induced and electrical control of the photoluminescence yield of monolayer WS2

Ricardo Javier Peña Román, Rémi Bretel, Delphine Pommier, Luis Enrique Parra Lopez, Étienne Lorchat, Elizabeth Boer-Duchemin, Gérald Dujardin, Andrei Borisov, Luiz Fernando Zagonel, Guillaume Schull, et al.

Tip-induced and electrical control of the photoluminescence yield of monolayer WS_2

Ricardo Javier Peña Román,[†,‖] Rémi Bretel,[‡,‖] Delphine Pommier,[‡,‖] Luis Enrique Parra López,[¶] Etienne Lorchat,[§] Elizabeth Boer-Duchemin,[‡] Gérald Dujardin,[‡] Andrei G. Borisov,[‡] Luiz Fernando Zagonel,[†] Guillaume Schull,[¶] Stéphane Berciaud,[¶] and Eric Le Moal[*,‡]

†*Institute of Physics "Gleb Wataghin", Department of Applied Physics, State University of Campinas-UNICAMP, 13083-859, Campinas, Brazil*

‡*Université Paris-Saclay, CNRS, Institut des Sciences Moléculaires d'Orsay, 91405, Orsay, France*

¶*Institut de Physique et de Chimie des Matériaux de Strasbourg, Université de Strasbourg, CNRS, IPCMS, UMR 7504, F-67000 Strasbourg, France*

§*NTT Research, Inc., Physics & Informatics (PHI) Laboratories, Sunnyvale, CA 94085, USA*

‖*These authors contributed equally to this work.*

E-mail: eric.le-moal@universite-paris-saclay.fr

Phone: +33 (0)1 69 15 66 97. Fax: +33 (0)1 69 15 67 77

Abstract

The photoluminescence (PL) of monolayer tungsten disulfide (WS_2) is locally and electrically controlled using the non-plasmonic tip and the tunneling current of a scanning tunneling microscope (STM). The spatial and spectral distribution of the emitted

light is determined using an optical microscope. When the STM tip is engaged, short-range PL quenching due to near-field electromagnetic effects is present, independent of the sign and value of the bias voltage applied to the tip-sample tunneling junction. In addition, a bias voltage-dependent long-range PL quenching is measured when the sample is positively biased. We explain these observations by considering the native n-doping of monolayer WS_2 and the charge carrier density gradients induced by electron tunneling in micrometer-scale areas around the tip position. The combination of wide-field PL microscopy and charge carrier injection using an STM opens up new ways of exploring the interplay between excitons and charge carriers in two-dimensional semiconductors.

Keywords

nano-optics, exciton, 2D materials, scanning tunneling microscopy

Monolayer transition-metal dichalcogenides (TMDs) are direct-bandgap two-dimensional (2D) semiconductors[1–7] that have potentially groundbreaking applications in nanodevice technologies thanks to their unique optical and electronic properties.[8–16] Even at room temperature, the photophysics of monolayer TMDs is governed by the exciton dynamics, i.e., the dynamics of bound electron-hole pairs that can diffuse in the 2D lattice and interact with each other or with charge carriers. Manipulating the elementary excitonic processes (i.e., exciton creation, diffusion and recombination) is key for the performance of TMD-based devices. In particular, the control of the luminescence quantum yield is a long sought-after goal in 2D optoelectronics and nanophotonics. Near-unity photoluminescence (PL) quantum yield has been obtained in monolayer TMDs by eliminating non-radiative defect-mediated recombinations through chemical passivation[17] or by neutralizing the excess charge carriers via electrostatic gating to prevent the formation of charged excitons (i.e., trions).[18] Attempts to control trion formation in monolayer TMDs on the nanoscale have been reported,[19] e.g., using laser-excited charge transfer plasmons in the plasmonic tip-substrate nanocavity of an

atomic force microscope.[20] Nevertheless, distinguishing charge injection and electromagnetic effects[21,22] in such plasmon-based experiments is challenging. Moreover, most of the techniques to locally control or excite excitons in 2D materials that are based on a scanning probe[20] (or a focused electron beam[23]) provide virtually no direct information about the diffusion and local recombination processes of these excitons, a key aspect for the integration of these materials in realistic devices.

In the present Letter, we report on the local electrical control of the PL quantum yield of monolayer WS_2 using the tip and current of a scanning tunneling microscope (STM). We combine STM and wide-field laser-induced PL microscopy in real space to demonstrate the reversible, bias and current-dependent modification of the PL quantum yield within a microscale area around the tip. All experiments are carried out under ambient conditions on monolayer WS_2 deposited on a transparent conducting substrate and using a non-plasmonic STM tip. At positive sample bias only and above a certain voltage threshold, long-range quenching is observed, whose spatial distribution is consistent with the injection and diffusion of charge carriers in the semiconductor. Based on PL spectroscopy, we demonstrate the link between this long-range quenching effect and the formation of trions, due to the local increase of the charge carrier density. At both negative and positive sample bias, a comparatively shorter-range quenching effect is observed, which is of electromagnetic origin. The results of this study open up new opportunities in TMD-based technology and in the use of STM combined with wide-field optical microscopy to investigate exciton physics in 2D semiconductors and their heterostructures on the nanoscale.

Figure 1(a) shows the experimental setup and the principle of the experiment. An air-operated STM head is mounted on top of an inverted optical microscope.[24] The STM tip is an electrochemically etched tungsten wire, i.e., a metal that does not support surface plasmons in the visible frequency range. Mechanically exfoliated WS_2 microflakes are deposited onto an indium-tin oxide (ITO)-coated glass coverslip (ITO thickness 85 nm) using a dry transfer method.[25] As shown in Fig. 1(b), the studied WS_2 microflakes are fragmented into several

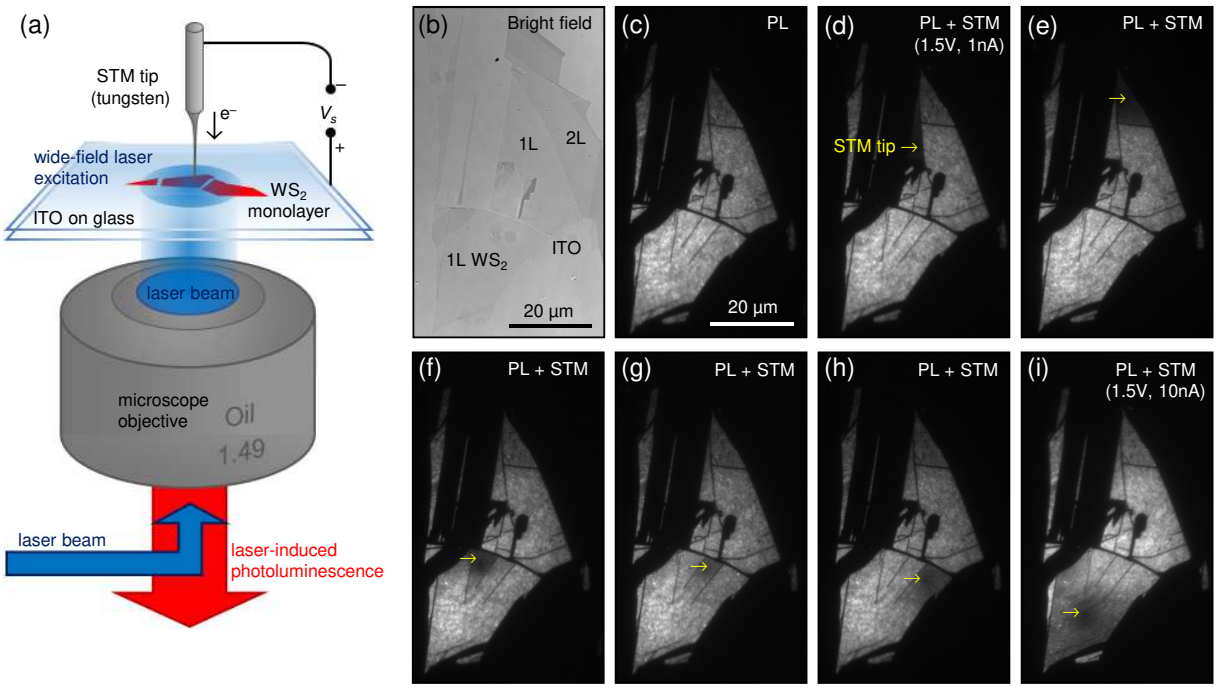

Figure 1: (a) Schematics of the experiment: the sample, i.e., a thin exfoliated WS_2 microflake on an ITO-coated glass coverslip, is placed between the tungsten tip of an STM and a high-NA oil immersion microscope objective. The PL of the sample is excited using a collimated laser beam (excitation wavelength $\lambda = 465.8$ nm, laser power about 1 μW, i.e., about 0.012 W cm^{-2} at the sample) in normal incidence through the substrate (episcopic illumination). The collected light is imaged on a CCD camera or on the entrance slit of a spectrometer (longpass filter from $\lambda = 491$ nm). (b) White light transmission microscopy image and [(c) to (i)] wide-field PL microscopy images of the same area of the sample. In (b), 1L and 2L designate mono and bilayer areas of the WS_2 microflake, respectively. The STM tip is vertically withdrawn several micrometers away from the surface in (c) and engaged, i.e., in the tunnel regime with closed feedback loop in (d) to (i). Arrows indicate the lateral position of the tip apex on the sample. The sample bias voltage is 1.5 V and the tunneling current setpoint is 1 nA in (c) to (h) and 10 nA in (i).

domains due to the exfoliation and transfer methods. In the PL image shown in Fig. 1(c), the monolayer areas of the WS_2 flakes are the bright areas, whereas the bilayer and thicker areas of the flakes are almost as dark as the bare substrate. This is because multilayer WS_2 has an indirect electronic bandgap. PL from the sample is excited using a continuous-wave argon-ion laser emitting at a wavelength of 465.8 nm, under wide-field episcopic illumination in normal incidence. The laser power at the sample is about 0.012 W cm^{-2}. The emitted light is collected through the substrate using an oil-immersion microscope objective of high numerical aperture (NA = 1.49). Taking into account the detection efficiency of our setup and the absorption coefficient of monolayer WS_2,[26] from the PL image shown in Fig. 1(c) we estimate that the radiative quantum yield of the sample in the absence of the STM tip is about 0.007 ± 0.003 (more details are available in Sec. S2 of the Supplementary Information). This result is in agreement with previous reports for monolayer WS_2 at room temperature.[18,27] In all the reported experiments, where the PL is detected with the STM tip engaged, the STM-induced electroluminescence (STML) of the sample[28] is undetected or negligible as compared to the detected PL signal. In particular, the STM-induced effects reported in this Letter are observed regardless of whether the bias voltage applied to the tip-sample junction is lower or higher than the STML onset voltage for this sample ($V_s \approx 1.8$ V),[29] which confirms that these effects are not due to STML (more data is available in Sec. S7 of the Supplementary Information).

Figures 1(d) to 1(i) show the results of experiments combining STM and wide-field laser-induced PL microscopy, where the PL images are recorded in presence of the STM tip (i.e., the STM is operating in constant current mode with the feedback loop closed). The effect of the biased tip-sample junction on the semiconductor PL quantum yield is spatially resolved in real space using the optical microscope. Here, the sample bias is positive, i.e., the tunneling electrons flow from the tip to the sample. Figs. 1(d) to 1(i) differ in the lateral position of the STM tip, which is kept fixed during the acquisition of each image (i.e., the tip is not scanning). This series of images reveals that the PL of a particular domain is partially

quenched when the STM tip is placed above it during the measurement. The observed effect extends spatially over an area of several tens (hundreds) of square micrometers for a setpoint current of 1 nA (10 nA). The effect does not spread to other neighboring flake domains. PL quenching is spatially limited by the edges or by internal cracks [see Figs. 1(f) to 1(h)] of the targeted flake domain. This suggests that the observed effect is governed by the diffusion of charge carriers in the WS_2 monolayer. Here, we rule out the possibility that the observed effect could result from "ionic gating".[30] By "ionic gating", we mean that the ions in a water layer adsorbed on top of the WS_2 monolayer or bridging the tip-sample junction act as a microscale electrode. Indeed, if such a water layer were short-circuiting the tip-sample junction, strong fluctuations of the STM current and tip-sample distance would be observed, especially at bias voltages exceeding the electrolysis potential of water.[31] Such an effect, however, is not experimentally observed (see Sec. S9). Most importantly, the PL quenching is reversible, since it disappears once the STM tip is withdrawn and the tunneling current stops flowing. Visibly, the PL of different areas of the same flake can successively be quenched and recovered. Further details about the data shown in Fig. 1 may be found in the Supplementary Information (see Secs. S1 and S3). Below, we analyze the bias and current dependence of this quenching effect.

A selection of PL images recorded on a monolayer WS_2 microflake is shown in chronological order in Figs. 2(a) to 2(e) (the status of the STM tip is specified at the top of the figures). The result of the complete experiment, i.e., a series of 80 images acquired at a rate of 1 frame s^{-1}, is presented in Figs. 2(f) and 2(g). During the PL measurement, the STM tip is engaged and the sample bias voltage is gradually increased from 0.5 to 1.5 V in steps of 0.1 V, before the tip is finally withdrawn. The PL intensity integrated over a circular area of radius ≈ 3 μm centered on the position of the tip is plotted in Fig. 2(f) versus time, together with the applied bias voltage. The PL intensity integrated over all in-plane directions is plotted versus the lateral distance from the tip in Fig. 2(g). In Figs. 2(f) and 2(g), the PL intensity is divided by its value at the beginning of the experiment; thus, it is

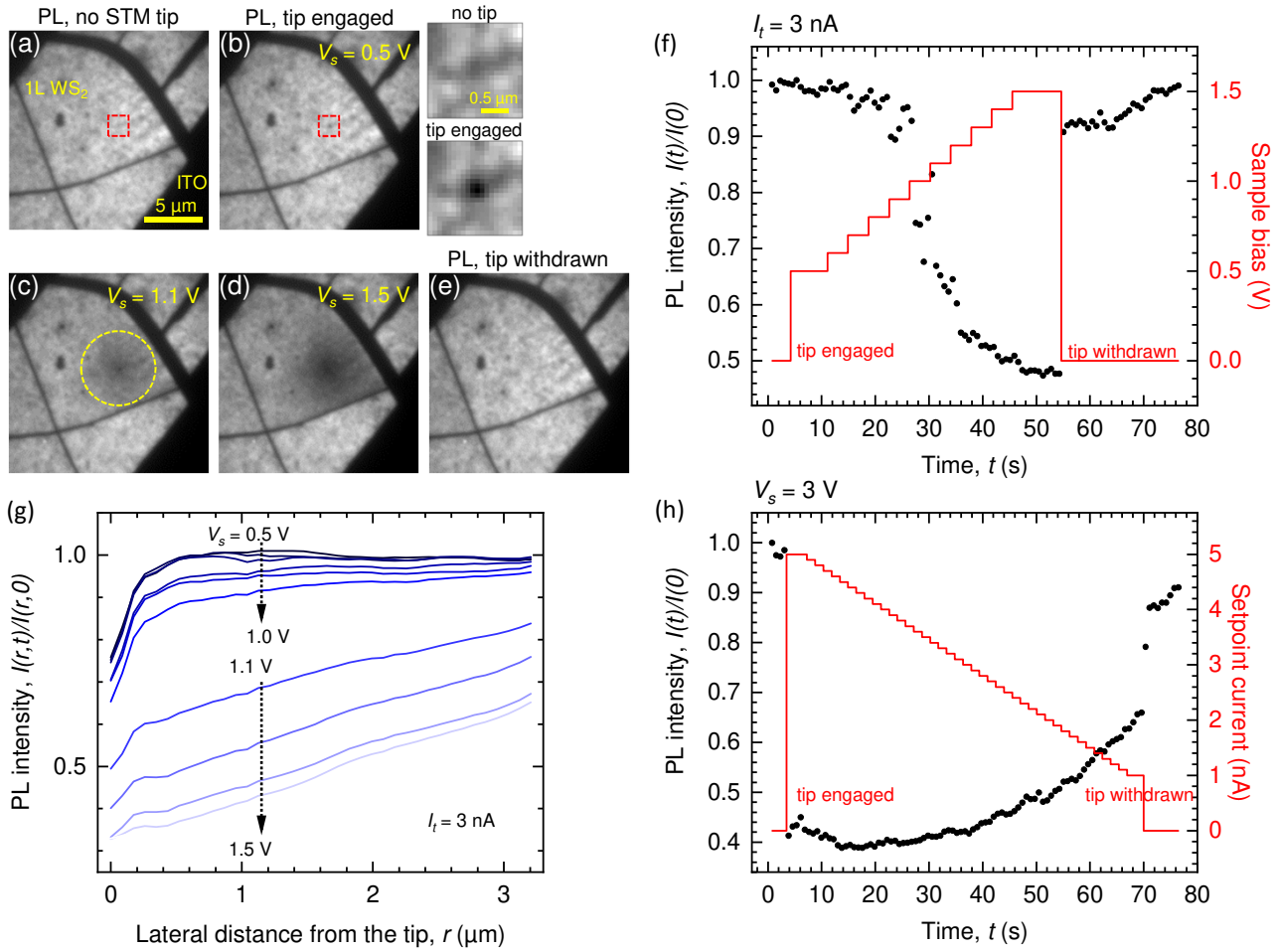

Figure 2: [(a) to (e)] Laser-induced PL microscopy images of a monolayer WS_2 microflake on ITO in absence (a and e) or presence (b to d) of the STM tip, with different bias voltages applied to tip-sample junction. The tunneling current setpoint is $I_t = 3$ nA. In the inset, the area designated by the red square in (a) and (b) is shown with a magnified scale. In (b), the tip is located in the center of the red square. In (c), the yellow circle is centered on the tip position and its radius is 3.2 μm. (f) PL intensity (black dots) averaged over the area designated by the yellow circle shown in (c) and STM bias voltage (red line) plotted versus time. (g) PL intensity radial profile, averaged over all in-plane directions, for various STM bias voltages. The PL intensity in (f) and (g) is taken from the same experiment as the images shown in (a) to (e), and is divided by its value measured at time $t = 0$. (h) PL intensity as in (f) and STM tunneling current setpoint (red line) versus time. The bias voltage is kept constant at $V_s = 3$ V.

the relative variation of the PL intensity that is considered, in order to get rid of all spatial heterogeneities. The zoomed-in areas shown in the inset of Fig. 2(b) and the top curves in Fig. 2(g) reveal that, at low bias voltage ($V_s \leq 0.8$ eV), the PL is quenched within a localized area around the tip. The resulting intensity dip has a full-width-at-half-maximum (FWHM) of 0.25 to 0.30 μm, which is slightly larger than the ideal point spread function (PSF) of the optical microscope ($\lambda_0/2\mathrm{NA} \approx 0.21$ μm).

Several physical effects, which only occur in the near field of the tip, may contribute to this "short-range" quenching. The effect of the strong electrostatic field in the biased tip-sample junction (on the order of volts per nanometers) and the modification of the dielectric screening of the excitons due to the presence of the tip may play a part. Due to the sharpness of the STM tip (i.e., its typical angular aperture and curvature radius are 15° and 30 nm, respectively[32]), such effects are expected to be localized within a nanoscale area under the tip apex. Foremost, due to the extreme proximity of the metallic tip (in the tunnel regime, the apex of the STM tip is at a distance of about 1 nm from the sample), ultrafast non-radiative energy transfer from the exciton to the tip is expected in the nanoscale region under the tip. Simple analytical calculations shown in the Supplementary Information (see Sec. S6) confirm that the presence of the tungsten tip in the near field of the 2D semiconductor opens up additional excitonic decay channels. These are almost entirely non-radiative within an area that extends over lateral distances that are comparable to the radius of curvature of the tip.

However, at higher bias voltage ($V_s \geq 1.1$ eV), the presence of the tip and the associated tunneling current yields a comparatively much larger, micrometer-sized, dark circular area. The resulting intensity dip increases both in depth and in lateral spread as the bias voltage is raised. At $V_s = 1.5$ eV [Fig. 2(d)], the PL averaged over a micrometer-scale area around the tip (i.e., a disk of radius 3.2 μm) is reduced by a factor of two as compared to result without the tip and tunneling current. As shown in Fig. 2(d), this "long-range" quenching effect does not extend across the cracks separating the split domains of the monolayer flake;

thus, it must be of electronic origin, i.e., related to the transport of charge carriers in the semiconductor. In Fig. 2(h), a similar experiment as that of Fig. 2(f) is carried out, where the bias voltage is kept at 3 V and the setpoint current is decreased stepwise from 5 to 1 nA. Visibly, when the electronic current flowing from the tip to sample is lower, the PL quenching is weaker. Figs. 2(f) and 2(h) also show that the PL fully recovers on a time scale of about 10 to 20 s after the withdrawal of the tip. This inertia is not detected in Fig. 1 due to the longer acquisition time used (120 s). These observations are confirmed by the additional data shown in the Supplementary Information (see Sec. S5).

The spatial distribution of the "long-range" quenching effect, its dependence on the tunneling current and its onset above a voltage threshold of about 1 V are consistent with the electronic doping of the part of the monolayer of WS_2 which is under the STM tip. This electronic doping is due to electron injection via tunneling from the tip into the conduction band of WS_2. Indeed, partial electronic decoupling of the WS_2 flake and the conducting substrate is very likely due to the presence of a nanometer-thin layer of adsorbed water between the substrate and the monolayer. The observation of such an interfacial water layer has been reported for various exfoliated 2D materials transferred to solid substrates and is unavoidable when samples are prepared in ambient conditions.[33–35] Thus, we expect that the STM tip produces a spatial gradient in the charge carrier density of the semiconductor in the area around the tip position. This may explain why the strength of the "long-range" quenching effect decreases with lateral distance from the STM tip. Within this hypothesis, the voltage threshold for the "long-range" quenching effect for positive sample bias corresponds to the voltage beyond which the Fermi level of the tip lies above the conduction band minimum of monolayer WS_2 on ITO. Indeed, beyond this voltage threshold, electrons can tunnel into the conduction band of the semiconductor, thus charging the WS_2/ITO system, which may act as a parallel-plate capacitor (more details about this interpretation provided in Sec. S4 of the Supplementary Information). Here, we assume that the electrons injected in the conduction band of the WS_2 monolayer may diffuse laterally in the semiconductor for distances on the

order of micrometers before they are evacuated in the underlying substrate.[36,37] Such long diffusions lengths are expected when the monolayer is partly decoupled from the substrate by a thin layer of water.[34] Below, we examine if similar behavior is observed at negative sample bias, i.e., when tunneling electrons flow from sample to tip.

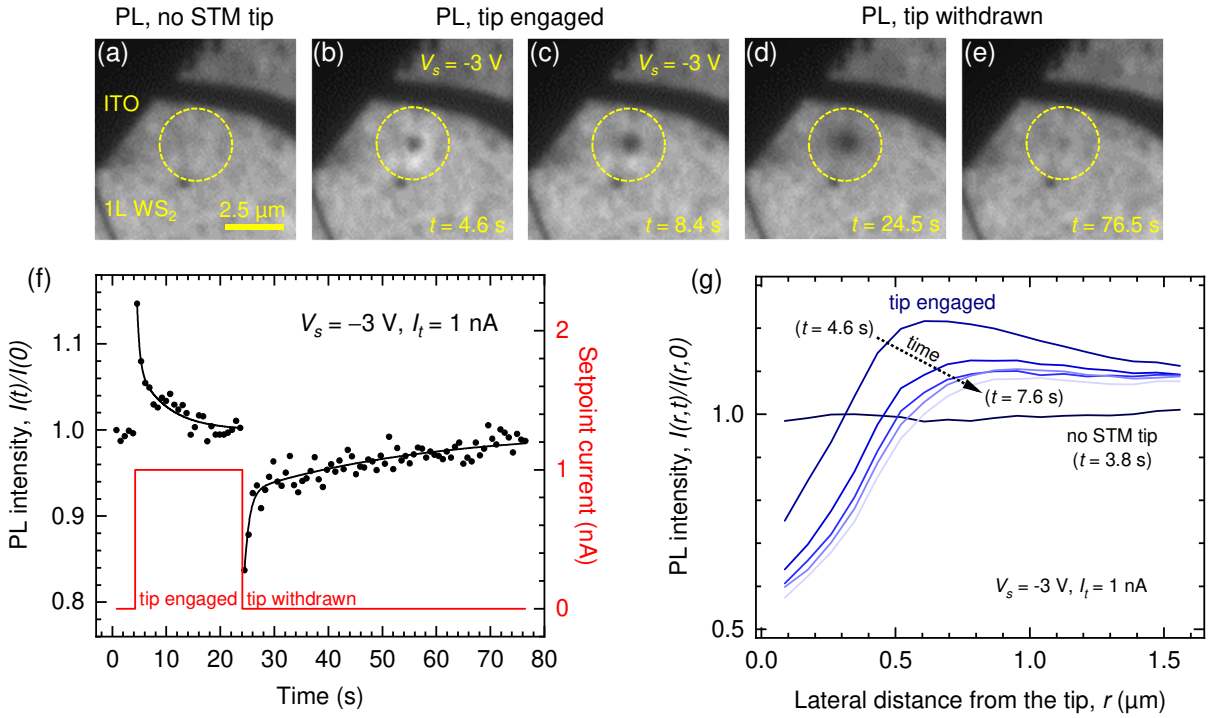

Figure 3: [(a) to (e)] Laser-induced PL microscopy images of a monolayer WS_2 microflake on ITO in the absence or presence of the STM tip, at negative sample bias $V_s = -3$ V ($I_t = 1$ nA). (f) PL intensity averaged over the area designated by a yellow circle in (a) to (e) (black dots) plotted versus time. Biexponential decay curves are fit to the data to guide the eye. The yellow circle in (a) to (e) is centered on the tip position and its radius is 1.55 μm. (g) PL intensity radial profile, averaged over all in-plane directions. The PL intensity in (f) and (g) is taken from the same experiment as the images in (a) to (e), and is divided by the value measured at time $t = 0$.

Figure 3 shows the results of an experiment similar to that introduced in Fig. 2, except that the sample is negatively biased. To simplify, we consider only one set of STM parameters (i.e., -3 V and 1 nA) and we focus on the spatial and temporal dynamics of the PL quantum yield modification. Quenching around the tip position is also observed at negative sample bias [see Figs. 3(a) to 3(e)]; however, its lateral extent around the tip is considerably smaller, i.e., typically less than 1 μm, as compared to that which was seen for positive sample

bias. Most remarkably, the radial intensity profiles shown in Fig. 3(g) reveal that, outside a submicrometer-scale area around the tip position where PL is quenched, the PL is actually enhanced by about 10%. The PL intensity variation averaged over a micrometer-scale area around the tip [see Fig. 3(f)] exhibits a time dependence that is reminiscent of the charging and discharging of a capacitor. PL enhancement and quenching of about 15% are transiently observed in Fig. 3(f) immediately after tip engagement and withdrawal, respectively; however, the averaged PL intensity tends to its initial value after a few tens of seconds.

The different behavior observed at negative sample bias as compared to positive bias may result from the natural doping of WS_2. Indeed, WS_2 is known to be inherently n-doped because of sulfur vacancies and WS_2-based transistors usually are unipolar devices.[38] Recent publications on monolayer WS_2 on ITO suggest that it is n-doped.[29,39] Electron injection via tunneling from the tip into the conduction band of the n-doped semiconductor will locally increase the density of majority charge carriers, whereas the inverse effect may be obtained if electrons tunnel from the sample to the tip. Thus, if higher charge carrier densities in the semiconductor yield stronger PL quenching, we expect a stronger quenching effect at positive as compared to negative sample bias. In other words, electron tunneling from the sample to the tip tends to compensate for the native doping of monolayer WS_2. Complementary results are available in the Supplementary Information (see Sec. S8), where we examine the effect of alternating positive and negative sample bias and futher demonstrate that the quenching is due to electron tunneling-induced doping of the semiconductor. Below, in order to elucidate the mechanisms behind the reported observations, we investigate bias-dependent modifications of the spectral PL distribution.

In what follows, we use the entrance slit of an imaging spectrometer to select the PL emitted from a narrow, micrometer-long band about the tip position. A series of PL spectra is measured in the same area of the sample (i.e., same lateral position of the STM tip) at various bias voltages. We successively measure the PL spectrum with the tip engaged and withdrawn, i.e., in tunnel regime with the feedback loop closed and retracted micrometers away from

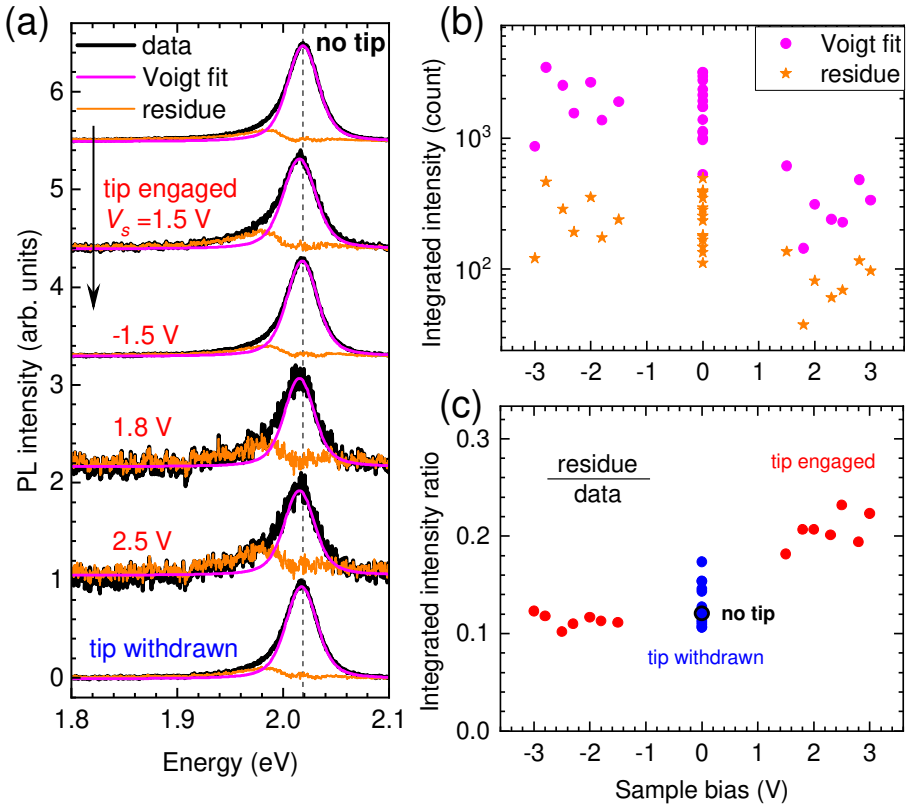

Figure 4: Spectral PL distribution and bias-dependence of the STM-induced effect. (a) selection of PL spectra of monolayer WS_2 measured in the same area of the sample, where the STM tip is either withdrawn or engaged, at various sample bias voltages. The chronological order of the measurements is from top to bottom and the first spectrum (labeled "no tip") is measured (with the tip withdrawn) before any STM manipulation of the area. The intensity of the PL spectra is normalized to unity. Data are fitted using a Voigt profile (magenta curve) and the fit residue is plotted on the same graph (orange curve). (b) Integrated areas under the curves of the fitted Voigt profile (magenta dots) and fit residue (orange stars) shown in (a), plotted versus sample bias voltage. (c) Ratio between the integrated areas under the curves of the fit residue and total emission spectrum, plotted versus sample bias voltage (black dot: before any STM manipulation, red dots: tip engaged, blue dots: tip withdrawn). Setpoint current is 3 nA for all the measurements involving the STM. PL: laser excitation at $\lambda = 465.8$ nm, longpass filter from $\lambda = 491$ nm.

the sample. We alternate positive and negative sample bias and increase the bias voltage after each sequence. Figure 4(a) shows a selection of the measured PL spectra, the intensity of which is normalized to unity. The PL spectrum measured before any STM manipulation (see data labeled "no tip") is well fitted using a single Voigt profile centered on 2.019 eV with a FWHM of 35 meV. This is typical of a thermally broadened radiative recombination of band-edge neutral excitons (A excitons) in monolayer WS_2 at room temperature. The fit residue, i.e., the data subtracted by the fit function, reveals an additional contribution on the low-energy side of the main peak, which is shifted by 32 ± 3 meV and features an exponential decay tail on its low-energy side. In previous studies, the latter contribution has been either ascribed to a broadening of the exciton peak due to phonon coupling[40,41] or the radiative recombination of trions, i.e., charged excitons.[5] Binding energies of 35 and 42 meV have been reported for triplet and singlet trions in monolayer WS_2,[42] respectively, and the asymmetry of the trionic PL peak has been related to the electron recoil effect.[43,44] If the fit residue in Fig. 4(a) is in fact due to trions, increasing the exciton-to-trion conversion rate should increase the "weight" of the fit residue in the total emission spectrum. Moreover, it has been reported that the dominant trion recombination pathway in a WS_2 monolayer at room temperature is non-radiative, whereas neutral exciton recombination is radiative.[18] Therefore, a reduction of the overall PL quantum yield of the semiconductor is also expected when more excitons are converted into trions.[36]

In the following, we determine if the electron tunneling-induced PL quenching effect observed in monolayer WS_2 is related to an increase of the conversion of excitons to trions. We apply the same fit procedure as described above to all PL spectra [see Fig. 4(a)] and we integrate the area under the Voigt profile and the fit residue over energy, in order to express these two contributions in terms of integrated PL. The absolute value of the integrated PL and the relative contribution of the fit residue are plotted as a function of the bias voltage in Fig. 4(b) and 4(c), respectively. In Fig. 4(c), we find that the relative contribution of the fit residue at negative sample bias almost equals that measured before any STM

manipulation, no matter the value of the bias voltage, and is increased by a factor of about 2 at positive sample bias. Thus, assuming that the fit residue is trionic emission, the electron tunneling-induced quenching of PL at positive sample bias indeed coincides with a relative increase in the contribution of trions, which is most likely due to the increased density of negative charge carriers in the semiconductor. Nonetheless, in terms of absolute value of the integrated PL, the trion PL contribution does not increase at the expense of the excitonic contribution; instead, both contributions decrease at positive sample bias [see Fig. 4(b)]. Thus, additional mechanisms on top of trion formation may be at play, which reduce the radiative quantum yield of neutral excitons. Such mechanisms may include the Auger-like non-radiative recombination of excitons, the rate of which is expected to increase with an increase in the density of charge carriers in the semiconductor.

In conclusion, we have introduced a new method to locally and electrically control the PL quantum yield of monolayer TMDs on transparent electrodes (i.e., ITO-coated glass) using an STM equiped with a tungsten tip. Via a combination of STM and wide-field PL microscopy, we uncover the effects of the biased tip-sample junction on the excitonic properties a WS_2 monolayer. The PL quantum yield is modified in two ways, both of which are shown to be reversible. First of all, the near-field electromagnetic non-radiative transfer of energy from excitons to the non-plasmonic tip quenches the PL in an almost diffraction-limited area just below the tip. Secondly, bias and current-dependent PL quenching and enhancement occur within micrometer-scale areas around the tip position. We ascribe such "long-range" effects to lateral spatial gradients in the charge carrier density in the monolayer, which presumably modify the relative PL contributions of neutral and charged excitons and the radiative quantum yield of excitons. Such doping gradients result from electron tunneling between the tip and the semiconductor and a partial electronic decoupling of the monolayer from the underlying conducting substrate. Future work may include the modeling of the charge carrier diffusion profile around the STM tip when it is engaged. This may require solving the drift-diffusion equations while including the lateral electronic

band bending induced by the biased tip-sample junction and by the tunneling current. It is noteworthy that local electrostatic gating due to the electric field in the biased tunnel junction and the local injection of charge carriers in the semiconductor are two effects that inevitably coexist in the STM experiments reported here. Nevertheless, we believe that the observation of a threshold bias voltage for the onset of long-range PL quenching is a strong indication that long-range PL quenching is governed by local charge carrier injection. Finally, the use of an STM tip as a nanoscale and scanning electrode in the wide-field PL microscopy of semiconductors opens up prospects for the study of the exciton and charge carrier interactions in more intricate TMD-based systems, e.g., strain and defect-engineered TMD layers or van der Waals heterostructures.[45,46]

Acknowledgement

This work is supported by public grants from the French National Research Agency (H2DH ANR-15-CE24-0016, Intelplan ANR-15-CE24-0020, M-Exc-ICO ANR-16-CE24-0003 and ATOEMS ANR-20-CE24-0010) and overseen by the ANR as part of the "Investissements d'Avenir" program (Labex NIE ANR-11-LABX-0058-NIE and Labex NanoSaclay ANR-10-LABX-0035). We acknowlege the StNano clean room staff for technical support. S.B. acknowledges support from the Indo-French Centre for the Promotion of Advanced Research (CEFIPRA) and from the Institut Universitaire de France (IUF). This project has received funding from the European Research Council (ERC) under the European Union's Horizon 2020 research and innovation program (grant agreement No 771850). This work of the Interdisciplinary Thematic Institute QMat, as part of the ITI 2021-2028 program of the University of Strasbourg, CNRS and Inserm, was supported by IdEx Unistra (ANR 10 IDEX 0002), and by SFRI STRAT'US project (ANR 20 SFRI 0012) and EUR QMAT ANR-17-EURE-0024 under the framework of the French Investments for the Future Program. This work has received financial support from the Fundação de Amparo à Pesquisa do Estado de São Paulo (FAPESP),

through projects 18/08543-7, 20/12480-0 and 14/23399-9.

Supporting Information Available

The following files are available free of charge.

- suppinfo.pdf: Extended data set used for Figure 1; Estimation of the PL quantum yield from Figure 1; Quantitative analysis of PL quenching; Estimation of the charge carrier density; Additional data on the bias voltage dependence for positive and negative polarities; Simplified theoretical model of the non-radiative energy transfer from the excitons to the tungsten tip; Evidence that the observed PL redshifts are not due to STM-induced luminescence of WS_2; Effect of alternating positive and negative sample bias; Evidence that "ionic gating" does not play a significant role.

References

(1) Mak, K. F.; Lee, C.; Hone, J.; Shan, J.; Heinz, T. F. Atomically Thin MoS_2: A New Direct-Gap Semiconductor. *Phys. Rev. Lett.* **2010**, *105*, 136805.

(2) Splendiani, A.; Sun, L.; Zhang, Y.; Li, T.; Kim, J.; Chim, C.-Y.; Galli, G.; Wang, F. Emerging Photoluminescence in Monolayer MoS_2. *Nano Lett.* **2010**, *10*, 1271–1275.

(3) Mak, K. F.; Shan, J. Photonics and optoelectronics of 2D semiconductor transition metal dichalcogenides. *Nat. Photonics* **2016**, *10*, 216.

(4) Brar, V. W.; Koltonow, A. R.; Huang, J. New Discoveries and Opportunities from Two-Dimensional Materials. *ACS Photonics* **2017**, *4*, 407–411.

(5) Wang, G.; Chernikov, A.; Glazov, M. M.; Heinz, T. F.; Marie, X.; Amand, T.; Urbaszek, B. Colloquium: Excitons in atomically thin transition metal dichalcogenides. *Rev. Mod. Phys.* **2018**, *90*, 021001.

(6) Brar, V. W.; Sherrott, M. C.; Jariwala, D. Emerging photonic architectures in two-dimensional opto-electronics. *Chem. Soc. Rev.* **2018**, *47*, 6824–6844.

(7) Lorchat, E.; Parra López, L. E.; Robert, C.; Lagarde, D.; Froehlicher, G.; Taniguchi, T.; Watanabe, K.; Marie, X.; Berciaud, S. Filtering the photoluminescence spectra of atomically thin semiconductors with graphene. *Nat. Nanotechnol.* **2020**, *15*, 283–288.

(8) Geim, A. K.; Grigorieva, I. V. Van der Waals heterostructures. *Nature* **2013**, *499*, 419.

(9) Cheng, R.; Li, D.; Zhou, H.; Wang, C.; Yin, A.; Jiang, S.; Liu, Y.; Chen, Y.; Huang, Y.; Duan, X. Electroluminescence and Photocurrent Generation from Atomically Sharp WSe_2/MoS_2 Heterojunction p-n Diodes. *Nano Lett.* **2014**, *14*, 5590–5597.

(10) Furchi, M. M.; Pospischil, A.; Libisch, F.; Burgdörfer, J.; Mueller, T. Photovoltaic Effect in an Electrically Tunable van der Waals Heterojunction. *Nano Lett.* **2014**, *14*, 4785–4791.

(11) Ross, J. S.; Klement, P.; Jones, A. M.; Ghimire, N. J.; Yan, J.; Mandrus, D. G.; Taniguchi, T.; Watanabe, K.; Kitamura, K.; Yao, W.; Cobden, D. H.; Xu, X. Electrically tunable excitonic light-emitting diodes based on monolayer WSe_2 p-n junctions. *Nat. Nanotechnol.* **2014**, *9*, 268.

(12) Akinwande, D.; Petrone, N.; Hone, J. Two-dimensional flexible nanoelectronics. *Nat. Commun.* **2014**, *5*, 5678.

(13) Clark, G.; Schaibley, J. R.; Ross, J.; Taniguchi, T.; Watanabe, K.; Hendrickson, J. R.; Mou, S.; Yao, W.; Xu, X. Single Defect Light-Emitting Diode in a van der Waals Heterostructure. *Nano Lett.* **2016**, *16*, 3944–3948.

(14) Jariwala, D.; Howell, S. L.; Chen, K.-S.; Kang, J.; Sangwan, V. K.; Filippone, S. A.; Turrisi, R.; Marks, T. J.; Lauhon, L. J.; Hersam, M. C. Hybrid, Gate-Tunable, van der Waals p-n Heterojunctions from Pentacene and MoS_2. *Nano Lett.* **2016**, *16*, 497–503.

(15) Liu, C.-H.; Clark, G.; Fryett, T.; Wu, S.; Zheng, J.; Hatami, F.; Xu, X.; Majumdar, A. Nanocavity Integrated van der Waals Heterostructure Light-Emitting Tunneling Diode. *Nano Lett.* **2017**, *17*, 200–205.

(16) Binder, J.; Withers, F.; Molas, M. R.; Faugeras, C.; Nogajewski, K.; Watanabe, K.; Taniguchi, T.; Kozikov, A.; Geim, A. K.; Novoselov, K. S.; Potemski, M. Sub-bandgap Voltage Electroluminescence and Magneto-oscillations in a WSe_2 Light-Emitting van der Waals Heterostructure. *Nano Lett.* **2017**, *17*, 1425–1430.

(17) Amani, M. et al. Near-unity photoluminescence quantum yield in MoS_2. *Science* **2015**, *350*, 1065–1068.

(18) Lien, D.-H.; Uddin, S. Z.; Yeh, M.; Amani, M.; Kim, H.; Ager, J. W.; Yablonovitch, E.; Javey, A. Electrical suppression of all nonradiative recombination pathways in monolayer semiconductors. *Science* **2019**, *364*, 468–471.

(19) Wen, B. et al. Ferroelectric-Driven Exciton and Trion Modulation in Monolayer Molybdenum and Tungsten Diselenides. *ACS Nano* **2019**, *13*, 5335–5343.

(20) He, Z.; Han, Z.; Yuan, J.; Sinyukov, A. M.; Eleuch, H.; Niu, C.; Zhang, Z.; Lou, J.; Hu, J.; Voronine, D. V.; Scully, M. O. Quantum plasmonic control of trions in a picocavity with monolayer WS_2. *Sci. Adv.* **2019**, *5*, eaau8763.

(21) Park, K.-D.; Khatib, O.; Kravtsov, V.; Clark, G.; Xu, X.; Raschke, M. B. Hybrid Tip-Enhanced Nanospectroscopy and Nanoimaging of Monolayer WSe_2 with Local Strain Control. *Nano Lett.* **2016**, *16*, 2621–2627.

(22) Park, K.-D.; Jiang, T.; Clark, G.; Xu, X.; Raschke, M. B. Radiative control of dark excitons at room temperature by nano-optical antenna-tip Purcell effect. *Nat. Nanotechnol.* **2018**, *13*, 59–64.

(23) Bonnet, N.; Lee, H. Y.; Shao, F.; Woo, S. Y.; Blazit, J.-D.; Watanabe, K.; Taniguchi, T.; Zobelli, A.; Stéphan, O.; Kociak, M.; Gradečak, S.; Tizei, L. H. G. Nanoscale Modification of WS_2 Trion Emission by Its Local Electromagnetic Environment. *Nano Lett.* **2021**, *21*, 10178–10185.

(24) Cao, S.; Le Moal, E.; Bigourdan, F.; Hugonin, J.-P.; Greffet, J.-J.; Drezet, A.; Huant, S.; Dujardin, G.; Boer-Duchemin, E. Revealing the spectral response of a plasmonic lens using low-energy electrons. *Phys. Rev. B* **2017**, *96*, 115419.

(25) Castellanos-Gomez, A.; Buscema, M.; Molenaar, R.; Singh, V.; Janssen, L.; Zant, H. S. J. v. d.; Steele, G. A. Deterministic transfer of two-dimensional materials by all-dry viscoelastic stamping. *2D Mater.* **2014**, *1*, 011002.

(26) Li, Y.; Chernikov, A.; Zhang, X.; Rigosi, A.; Hill, H. M.; van der Zande, A. M.; Chenet, D. A.; Shih, E.-M.; Hone, J.; Heinz, T. F. Measurement of the optical dielectric function of monolayer transition-metal dichalcogenides: MoS_2, $MoSe_2$, WS_2, and WSe_2. *Phys. Rev. B* **2014**, *90*, 205422.

(27) Mohamed, N. B.; Lim, H. E.; Wang, F.; Koirala, S.; Mouri, S.; Shinokita, K.; Miyauchi, Y.; Matsuda, K. Long radiative lifetimes of excitons in monolayer transition-metal dichalcogenides $MX_2(M = Mo, W; X = S, Se)$. *Appl. Phys. Express* **2017**, *11*, 015201.

(28) Pommier, D.; Bretel, R.; Parra López, L. E.; Fabre, F.; Mayne, A.; Boer-Duchemin, E.; Dujardin, G.; Schull, G.; Berciaud, S.; Le Moal, E. Scanning Tunneling Microscope-Induced Excitonic Luminescence of a Two-Dimensional Semiconductor. *Phys. Rev. Lett.* **2019**, *123*, 027402.

(29) Peña Román, R. J.; Pommier, D.; Bretel, R.; Parra López, L. E.; Lorchat, E.; Chaste, J.; Ouerghi, A.; Le Moal, S.; Boer-Duchemin, E.; Dujardin, G.; Borisov, A. G.; Zagonel, L. F.; Schull, G.; Berciaud, S.; Le Moal, E. Electroluminescence of monolayer

WS_2 in a scanning tunneling microscope: Effect of bias polarity on spectral and angular distribution of emitted light. *Phys. Rev. B* **2022**, *106*, 085419.

(30) Gutiérrez-Lezama, I.; Ubrig, N.; Ponomarev, E.; Morpurgo, A. F. Ionic gate spectroscopy of 2D semiconductors. *Nat. Rev. Phys.* **2021**, *3*, 508–519.

(31) Rogez, B.; Cao, S.; Dujardin, G.; Comtet, G.; Le Moal, E.; Mayne, A.; Boer-Duchemin, E. The mechanism of light emission from a scanning tunnelling microscope operating in air. *Nanotechnology* **2016**, *27*, 465201.

(32) Le Moal, E.; Marguet, S.; Rogez, B.; Mukherjee, S.; Dos Santos, P.; Boer-Duchemin, E.; Comtet, G.; Dujardin, G. An Electrically Excited Nanoscale Light Source with Active Angular Control of the Emitted Light. *Nano Lett.* **2013**, *13*, 4198–4205.

(33) Li, Q.; Song, J.; Besenbacher, F.; Dong, M. Two-Dimensional Material Confined Water. *Acc. Chem. Res.* **2015**, *48*, 119–127.

(34) Peña Román, R. J.; Auad, Y.; Grasso, L.; Alvarez, F.; Barcelos, I. D.; Zagonel, L. F. Tunneling-current-induced local excitonic luminescence in p-doped WSe_2 monolayers. *Nanoscale* **2020**, *12*, 13460–13470.

(35) Ma, Y.; Kalt, R. A.; Stemmer, A. Local strain and tunneling current modulate excitonic luminescence in MoS2 monolayers. *RSC Adv.* **2022**, *12*, 24922–24929.

(36) Godiksen, R. H.; Wang, S.; Raziman, T. V.; Guimaraes, M. H. D.; Rivas, J. G.; Curto, A. G. Correlated Exciton Fluctuations in a Two-Dimensional Semiconductor on a Metal. *Nano Lett.* **2020**, *20*, 4829–4836.

(37) Ren, L.; Lombez, L.; Robert, C.; Beret, D.; Lagarde, D.; Urbaszek, B.; Renucci, P.; Taniguchi, T.; Watanabe, K.; Crooker, S. A.; Marie, X. Optical Detection of Long Electron Spin Transport Lengths in a Monolayer Semiconductor. *Phys. Rev. Lett.* **2022**, *129*, 027402.

(38) Schulman, D. S.; Arnold, A. J.; Das, S. Contact engineering for 2D materials and devices. *Chem. Soc. Rev.* **2018**, *47*, 3037–3058.

(39) Morozov, S.; Wolff, C.; Mortensen, N. A. Room-Temperature Low-Voltage Control of Excitonic Emission in Transition Metal Dichalcogenide Monolayers. *Adv. Opt. Mater.* **2021**, *9*, 2101305.

(40) Christiansen, D.; Selig, M.; Berghäuser, G.; Schmidt, R.; Niehues, I.; Schneider, R.; Arora, A.; de Vasconcellos, S. M.; Bratschitsch, R.; Malic, E.; Knorr, A. Phonon Sidebands in Monolayer Transition Metal Dichalcogenides. *Phys. Rev. Lett.* **2017**, *119*, 187402.

(41) Niehues, I. et al. Strain Control of Exciton-Phonon Coupling in Atomically Thin Semiconductors. *Nano Lett.* **2018**, *18*, 1751–1757.

(42) Jadczak, J.; Bryja, L.; Kutrowska-Girzycka, J.; Kapuściński, P.; Bieniek, M.; Huang, Y.-S.; Hawrylak, P. Room temperature multi-phonon upconversion photoluminescence in monolayer semiconductor WS_2. *Nat. Commun.* **2019**, *10*, 107.

(43) Esser, A.; Zimmermann, R.; Runge, E. Theory of Trion Spectra in Semiconductor Nanostructures. *physica status solidi (b)* **2001**, *227*, 317–330.

(44) Ross, J. S.; Wu, S.; Yu, H.; Ghimire, N. J.; Jones, A. M.; Aivazian, G.; Yan, J.; Mandrus, D. G.; Xiao, D.; Yao, W.; Xu, X. Electrical control of neutral and charged excitons in a monolayer semiconductor. *Nat. Commun.* **2013**, *4*, 1474.

(45) Zhang, S. et al. Nano-spectroscopy of excitons in atomically thin transition metal dichalcogenides. *Nat. Commun.* **2022**, *13*, 542.

(46) Mogi, H.; Arashida, Y.; Kikuchi, R.; Mizuno, R.; Wakabayashi, J.; Wada, N.; Miyata, Y.; Taninaka, A.; Yoshida, S.; Takeuchi, O.; Shigekawa, H. Ultrafast nanoscale

exciton dynamics via laser-combined scanning tunneling microscopy in atomically thin materials. *npj 2D Mater. Appl.* **2022**, *6*, 72.

Graphical TOC Entry